

Characterization of premixed swirling methane/air diffusion flame through filtered Rayleigh scattering

Meng Li(李猛), Bo Yan(闫博), Shuang Chen(陈爽), Li Chen(陈力), and Jin-He Mu(母金河)
Citation: Chin. Phys. B, 2022, 31 (**3**): 034702. DOI: 10.1088/1674-1056/ac2485
Journal homepage: http://cpb.iphy.ac.cn; http://iopscience.iop.org/cpb

What follows is a list of articles you may be interested in

Effect of pressure on the electrical properties of flexible NiPc thin films fabricated by rubbing-in technology

Khasan S Karimov, Fahmi F Muhammadsharif, Zubair Ahmad, M Muqeet Rehman, and Rashid Ali
Chin. Phys. B, 2021, 30 (**1**): 014703. DOI: 10.1088/1674-1056/abb3ec

Quantitative temperature imaging at elevated pressures and in a confined space with CH_4/air laminar flames by filtered Rayleigh scattering

Bo Yan(闫博), Li Chen(陈力), Meng Li(李猛), Shuang Chen(陈爽), Cheng Gong(龚诚), Fu-Rong Yang(杨富荣), Yun-Gang Wu(吴运刚), Jiang-Ning Zhou(周江宁), Jin-He Mu(母金河)
Chin. Phys. B, 2020, 29 (**2**): 024701. DOI: 10.1088/1674-1056/ab5f00

Effects of heat loss and viscosity friction at walls on flame acceleration and deflagration to detonation transition

Jin Huang(黄金), Wenhu Han(韩文虎), Xiangyu Gao(高向宇), Cheng Wang(王成)
Chin. Phys. B, 2019, 28 (**7**): 074704. DOI: 10.1088/1674-1056/28/7/074704

Physical and chemical effects of phosphorus-containing compounds on laminar premixed flame

Yongfeng Yin(殷永丰), Yong Jiang(蒋勇), Rong Qiu(邱榕), Caiyi Xiong(熊才溢)
Chin. Phys. B, 2018, 27 (**9**): 094701. DOI: 10.1088/1674-1056/27/9/094701

The dynamic characteristics of a valve-less micropump

Jiang Dan, Li Song-Jing
Chin. Phys. B, 2012, 21 (**7**): 074701. DOI: 10.1088/1674-1056/21/7/074701

Characterization of premixed swirling methane/air diffusion flame through filtered Rayleigh scattering

Meng Li(李猛)[1], Bo Yan(闫博)[1,2], Shuang Chen(陈爽)[1], Li Chen(陈力)[1,†], and Jin-He Mu(母金河)[1]

[1] *State Key Laboratory of Aerodynamics, China Aerodynamics Research and Development Center, Mianyang* 621000, *China*
[2] *Science and Technology on Scramjet Laboratory, National University of Defense Technology, Changsha* 410073, *China*

(Received 31 July 2021; revised manuscript received 27 August 2021; accepted manuscript online 8 September 2021)

Characteristics of a premixed, swirl methane/air diffusion flame at atmospheric pressure are measured by filtered Rayleigh scattering (FRS). Three operating conditions are investigated with the equivalence ratios of the methane/air flame covering a range of 0.67–0.83. Under each condition, single-shot and averaged FRS images over a region measured 39.3×65.6 mm^2 at seven cross sections of the flame are collected to demonstrate the flame behavior. A gradient calculation algorithm is applied to identify reaction zone locations and structures in the instantaneous FRS measurements. Statistical analysis for the mean FRS measurements is performed by means of joint probability density functions. The experimental results indicate that thermochemical state of the swirl flame is strongly influenced by equivalence ratio, leading to varieties of flame structures and temperature distributions. The gradient of the instantaneous FRS images clearly illustrates the characteristics of the reaction zone. The results also demonstrate that FRS can provide detailed insights into the behavior of turbulent flames.

Keywords: filtered Rayleigh scattering, equivalence ratio, swirl flame, temperature measurement

PACS: 47.80.Fg, 47.70.Pq, 47.80.Jk, 33.20.Fb **DOI:** 10.1088/1674-1056/ac2485

1. Introduction

Premixed swirl combustion is the most commonly used flame stabilization strategy in aero engines and gas turbines. The flame stabilization is achieved mainly by hot combustion products transported back to the inner recirculation zone (IRZ) of flame field.[1–4] However, premixed swirl flames are susceptible to instabilities in the form of thermoacoustic oscillations or unstable re-ignition.[5–8] These instabilities would lead to fierce disturbances in the combustion field and even destruction of system structures. Currently, the instabilities driven by the chemical mechanism are not well understood yet.[3,9]

To get a deeper insight into the mechanism of the premixed swirl combustion, laser-based techniques have been applied to study the correlations between dynamics of the flow field and flame structure. For instance, velocity measurement techniques such as laser Doppler velocimetry (LDV) and particle image velocimetry (PIV) were used to study the flow field of swirl flames.[1,3,10–13] The joint probability density functions (PDFs) of mixture fractions and major species concentrations were studied by laser Raman scattering.[1–4] For characterization of flame features, planer laser induced fluorescence (PLIF) of OH radicals, CH and OH* chemiluminescence imaging were used for front structures,[2,3,11,12,14] visualization of the reaction zones,[1] and heat release rate.[3,14]

Besides these flame parameters mentioned before, one scalar that is of particular importance in swirl combustion community is the temperature field, which yields the combustion processes including chemical reaction, heat transfer and gas expansion.[15] In the field of temperature measurements, laser-based thermometry techniques include filtered Rayleigh scattering (FRS), planer laser-induced fluorescence (PLIF), coherent anti-Stokes Raman scattering (CARS) and absorption-based approaches.[16,17] Among these approaches, FRS is a frequently used thermometry technique due to its ascendant capability of two-dimensional temperature distributions and instantaneous features.[18–31] Another benefit of FRS thermometry is that it can be applied in confined combustion environment. This is realized by absorption bands from atomic or molecular vapors, which can effectively remove the unwanted surface reflection scattering.[26]

Generally, intensity of detected FRS signal depends on the number density of the local mixture and the mole fraction-weighted differential Rayleigh scattering cross section. However, extracting temperature accurately from Rayleigh scattering is difficult because the number of species present is too large and changes in space and time due to reaction, mixing and diffusion.[27,28] In premixed combustion environments, there are mainly three methods to circumvent this problem, which are (1) simulating the local species through computational codes coupling equilibrium equations,[18] (2) using a particular fuel combination such that the mixture-averaged differential Rayleigh scattering section is nearly constant across composition space,[29–31] and (3) assuming that the scattering is from N_2 only.[18–23] The last approach is commonly taken under premixed methane-air combustion conditions when the equivalence ratio is less than 1.

[†]Corresponding author. E-mail: chenli_03@163.com

© 2022 Chinese Physical Society and IOP Publishing Ltd

The present study investigates the characteristics of a premixed turbulent methane/air diffusion flame in a typical swirl burner, which is operated under three equivalence ratio (Φ) conditions. The work employs FRS thermometry at a repletion rate of 10 Hz, providing a large interrogation field of view (39.3×65.6 mm^2) across the flame combustion field. The instantaneous and mean temperature field of the swirl flame at seven cross sections are measured allowing a detailed description and analysis of the flame features. Based on these measurement results, the gradients of instantaneous FRS images are calculated to demonstrate the shape, location and intensity of the reaction zone. Statistical analysis for the mean FRS measurements is also performed by means of joint probability density functions (PDFs).

2. Theoretical description

Figure 1 shows the spectrum of a combustion zone illuminated by a narrow linewidth light source. The molecular Rayleigh scattering spectrum (black line) has a bandwidth of several gigahertz based on broadening mechanisms related to the molecular motion, while the surface/particle scattering profile (blue line) has the same linewidth as the incident laser. Iodine makes a suitable filter since its spectral acts as an excellent medium for attenuating surface/particle scattering, but transmitting a portion of the Rayleigh scattering signal. The FRS signal collected by the detector is a superposition of iodine transmission curve and Rayleigh scattering spectrum of the observed volume element.

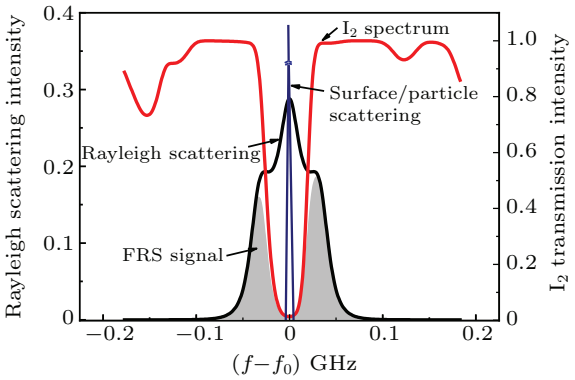


Fig. 1. Scheme of the FRS working principle: the surface/particle scattering (blue line) is absorbed by the I_2 molecular filter (red line), while portion of the FRS signal (gray area) passes through and is collected by the detector.

The FRS intensity collected by each pixel of a detector is the function of gas pressure P, gas temperature T, observation angle θ, the flow velocity $\boldsymbol{V}$ and the versus frequency v_{versus}. The Rayleigh scattering spectrum is calculated by employing the Tenti S6 lineshape model,[32] which is considered to be the most commonly used and accurate model for diatomic molecules.[33] The measured FRS intensity for a single species i is expressed as[34,35]

$$S_{\text{FRS,sf}} = cI_0 n \sum_i \varphi_i \Gamma_i, \tag{1}$$

where C is a constant representing the efficiency of the collection optics and imaging system, I_0 is the incident laser intensity, n is the gas number density, φ_i is the mole fraction, and Γ_i is a parameter specific to FRS written as

$$\Gamma_i = \left(\frac{\partial\sigma}{\partial\Omega}\right)_i \int_{-\infty}^{\infty} \tau_{\text{I}_2}(v)\cdot R_i(P,T,\boldsymbol{V},\theta;v_{\text{versus}})\,\mathrm{d}v. \tag{2}$$

Here, $(\partial\sigma/\partial\Omega)$ is the differential Rayleigh scattering cross section for species i, τ_{I_2} is the transmission spectra profile for the iodine filter, R_i is the RBS spectral profile for species i, and $v_{\text{versus}} = v - v_0 - v$ is the versus frequency referred to the central frequency v_0 of the incident laser; v is the Doppler frequency shift dealing with $\boldsymbol{V}$ and θ.

For methane-fuel premixed flames burning at atmospheric pressure with low fuel velocities ($|\boldsymbol{V}| < 100$ m/s) and low equivalence ratio ($\Phi < 1$), the local mixture-averaged differential scattering cross section term in the S6 model is nearly constant. Thus, the variations of the parameter Γ_i are not large in composition space and the Rayleigh scattering lineshape could be determined by N_2 only ($\varphi_{\text{N}_2} = 1$).[18–23] In publication,[19] the overall uncertainties in temperature due to the $\varphi_{\text{N}_2} = 1$ assumption and errors associated with other variables was approximately 2.5%–4.4% in the reacting regions of the flame. However, in the reactant region of the flame, the overall uncertainties raised to 11%–34% (respective equivalence ratio: 0.65–1.2), and the higher equivalence ratio resulted in the higher uncertainty. The results presented in our previous work[37] show that the overall deviation between FRS and the thermocouple is lower than 7% in the reacting region, which verifies the applicable usage of $\varphi_{\text{N}_2} = 1$ assumption in premixed lean methane/air flames. Therefore, the Rayleigh scattering lineshape of the investigated flame is determined by N_2 throughout this paper.

Excluding the dependences on C, I, n by dividing Eq. (1) with the referenced FRS measurement of quiescent air at ambient pressure, Eq. (1) can be rewritten to the equation for temperature with respect to the normalized FRS signal intensity parameter $S_{\text{FRS,sf}}/S_{\text{FRS,air}}$ as

$$T = T_{\text{air}} \cdot \frac{S_{\text{FRS,air}}}{S_{\text{FRS,sf}}} \cdot \frac{\sum_i \varphi_i \Gamma_i}{\Gamma_{\text{N}_2}}. \tag{3}$$

3. Experimental setup and flames

A general schematic of the experimental setup is shown in Fig. 2(a). The laser source for the measurement is an injection-seeded, frequency doubled, Q-switched, Nd:YAG laser operating at 532 nm with approximately 500 mJ per pulse. The laser has a pulse duration of 10 ns with a repetition rate of 10 Hz. Before passing through the sheet forming lens, a small portion of the laser beam was sent into a spectrometer (SM) to monitor the wavenumber for each incident laser pulse. Then

the incident laser beam was transformed into a light sheet by means of the sheet forming lens. Afterwards, the laser sheet was directed towards the test area and was aligned propagating parallel to the surface through the axis of the dual-annular nozzle. The laser sheet was approximately 0.5 mm thick (FWHM) with a height of 30 mm. The swirl generator inside the nozzle had a swirl number of 0.884. The exit surface of the central nozzle was defined as $h = 0$ for all measurements. The arrangement of the positions of the investigated cross sections is displayed in Fig. 2(b). By controlling the electric mobile platform, the laser sheet was successively overlapped with the seven cross sections (S) of the swirl flame, which were placed parallel to each other with an adjacent separation distance of 5 mm. The negative signs of the interrogation cross sections represent the direction towards the ICCD camera.

A major element of the FRS system is the I_2 filter. The I_2 filter is simply a glass cylinder in length 280 mm and diameter 70 mm with flat optical windows on both sides, which was used to absorb the surface/particle scattering from the collected signal. A high transmission 532 nm bandpass filter with 1 nm FWHM was placed between the I_2 filter and the ICCD camera to reduce any extraneous lights. The camera has a maximum resolution of 512×2048 pixel elements. The interrogation temperature fields consist of 480×800 pixel elements (39.3×65.6 mm^2) with a resolution of 0.08 mm. The timing of the ICCD camera and the laser was controlled by a DG535 delay generator. The investigated flame conditions are displayed in Table 1. The air and methane flows were controlled by electronic mass flow controllers. The equivalence ratio was calculated from the flow rates of air and methane.

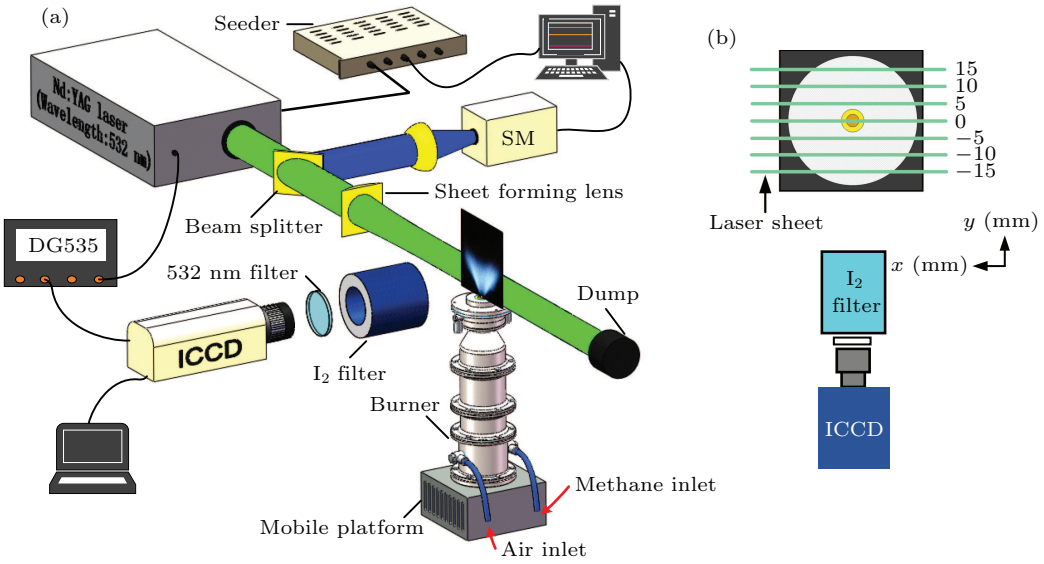


Fig. 2. (a) Schematic of experimental setup for FRS temperature measurements and (b) arrangement of the positions of the investigated cross sections.

Table 1. Investigated flames.

Flame	$Q_{methane}$ (L/min)	Q_{air} (L/min)	Equivalence ratio Φ	Investigated cross sections S						
1	2.8	40	0.67	–15	–10	–5	0	5	10	15
2	3.2	40	0.76	–15	–10	–5	0	5	10	15
3	3.5	40	0.83	–15	–10	–5	0	5	10	15

4. Results and discussion

4.1. Single-shot FRS measurements

Figure 3 shows the exemplary single-shot topologies at the investigated cross sections under three equivalence ratio conditions (listed in Table 1). The horizontal axis represents the uniform radius (r) of the flames while the vertical axis is the distance above the burner surface. In the single-shot FRS measurements, an absolute wavenumber fluctuation larger than 0.001 cm^{-1} from the central wavenumber of the I_2 absorption band was removed and was not considered in the results. For each flame, fifty FRS images were measured in unburnt methane/air mixture with the same flow flux to work as the reference condition for normalization according to Eq. (3). The normalized FRS images were median filtered by means of a 5×5 kernel to decrease the effect of measurement noise.

As seen in Fig. 3, it is obvious that the equivalence ratio strongly influences the temperature distribution and structure of the flames. Since the flame roots were lifted and the combustion were taking place at around $h = 8$ mm, the vertical axes of all FRS images were started at 8 mm. For all flames investigated, there were vortices rolling on the verge of the flame structure, reflecting the turbulent nature of the combustion field. The vortices at downstream locations were affected by the gradual increase of the shear layer instability, and eventually broken down and extricated from the main flame.

At lower equivalence ratio, the flame shape became narrower and the overall temperature intensity of the flame was lower, as expected. When the equivalence ratio was too low, i.e., $\Phi = 0.67$, the temperature distributions in S −15 and S 15 of flame 1 were almost invisible. In the marginal region spanning from S 15 to S 10 and S −10 to S −15, the flames collapsed due to the strong turbulence. This was demonstrated by a great number of structural change observed from one pulse to another in the 10 Hz instantaneous single-shot FRS measurements. An interest feature is that the shapes of flame structures in S 10 and S 15 mainly pointed towards left, while in S −10 and S −15, flame structures oriented right. The result corresponds, of course, to the helical mode of the combustion filed yielded by the swirl generator.

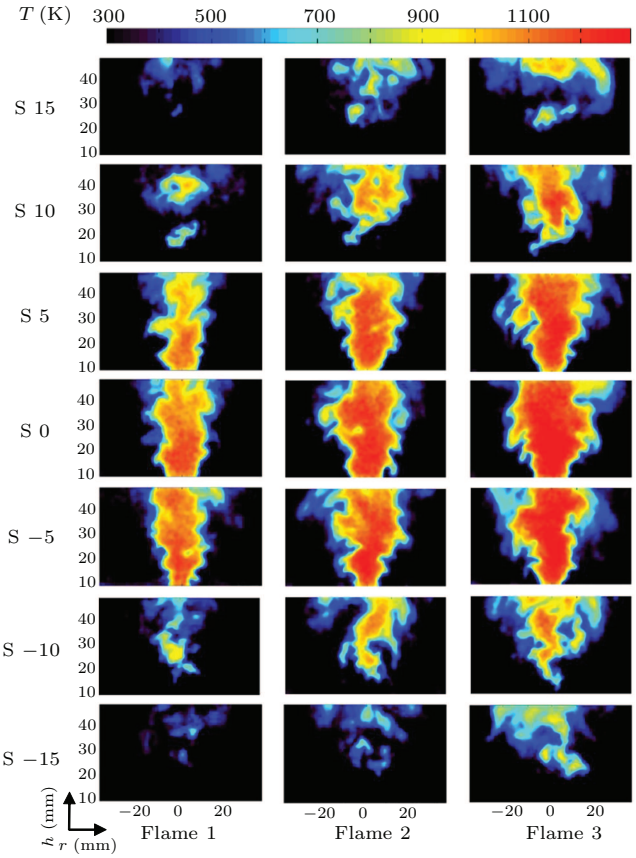


Fig. 3. Instantaneous FRS temperature measurements of flame 1–3.

A key parameter of interest in studying turbulent flames in the spatial position of the reaction zone. In order to reveal the instantaneous reaction zone characteristics of the investigated flames, a MATLAB algorithm was developed to calculate the gradient of the temperature intensity of each image in Fig. 3. As the local temperature was related to the thermochemical state of the swirl flame, its gradient could clearly and closely mark the location of the thermal reaction zone.[36] From this, the MATLAB algorithm incrementally scaned each pixel in each FRS image to compute its gradient intensity. The gradient of one pixel (x, y) was calculated as the root-mean-square SSD (sum of square of the difference) of the temperature difference between pixel $(x-1, y)$ and $(x+1, y)$ in the same row as well as the temperature difference between pixel $(x, y-1)$ and $(x, y+1)$ in the same column. Since the incident laser sheet has a thickness (FWHM) of around 0.5 mm, the temperature gradient is the integral over the thickness region of the laser sheet, extending the reaction zone up to a bigger scale than the actual situation. In addition, as a 5×5 median operator has been performed to the instantaneous FRS images for reducing measurement noise, it decreases the temperature differences between adjacent pixels, leading to lower gradient intensities. However, under the present condition, the effects of the laser sheet thickness scale and the median operator scale could be negligible regarding to the flame scale consisting of 480×800 pixel elements (39.3×65.6 mm).

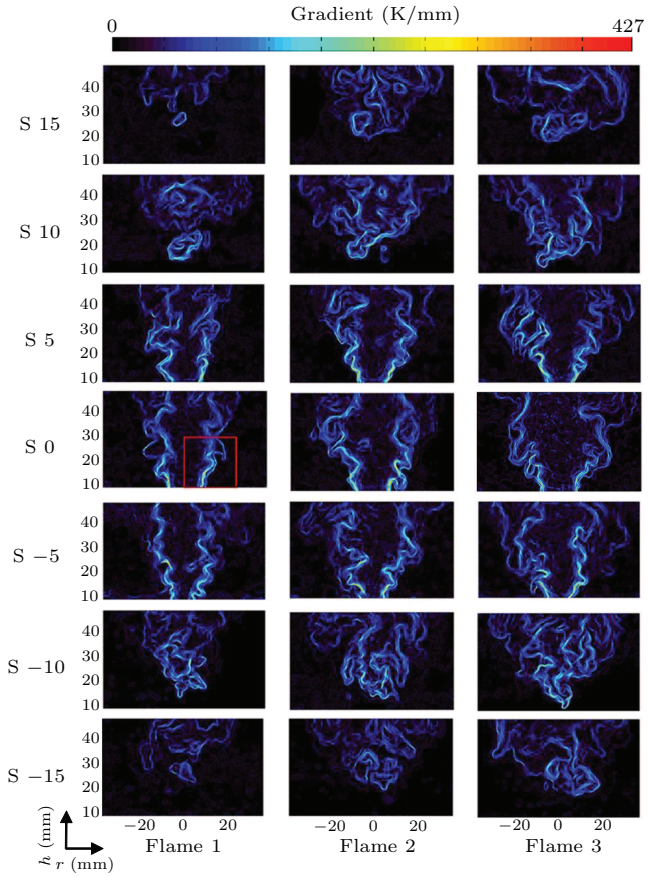


Fig. 4. Gradient of intensity of the instantaneous FRS temperature measurements in seven cross sections of flame 1–3.

Figure 4 shows the gradient of the instantaneous FRS temperature images from Fig. 3. All the flames show approximate rotational symmetric distribution around the burner axis of the reaction zone. The reaction zones of flame 1–3 mainly exhibit in the flame boundary regions, where the reaction zones oscillate rapidly and stochastically due to the strong turbulence, resulting in large positive and negative reaction zone curvature. Since the local temperature reflects the thermochemical state of the swirl flame, the gradient of temperature is an effective marker of the heat release tendency.

In S 0, strong temperature gradients take place in the district close to the flame root. The result indicates the presence of a helical processing vortex core (PVC), which is normally located in the flame boundary region between the stream of fresh gas and the recirculating burned mixture.[3,11,38] For a deeper insight into the reaction zone, a region (red box) in the central cross sections of flame 1–3 at a uniform radius r between 0 mm and 20.5 mm and an axial distance h between 0 mm and 20.5 mm are chosen to explore the heat release features, as shown in Fig. 5. It is obvious that the gradient has lower intensity and orient more randomly in the outer regions of the reaction zone, which differs from the gradient of the reaction zone. The direction of the latter definitely point to the inner side of the reaction zone, except in these areas coupled to the vortices in the azimuthal direction. The vortices affect the flame through flame rolling-up and local change of heat release. Taken together, the gradient of the instantaneous FRS results can demonstrate the heat release characteristics and the reaction zone distributions of the investigated flames.

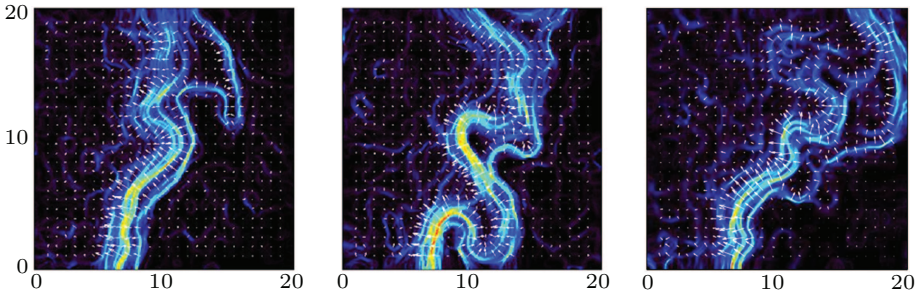


Fig. 5. Gradient distributions of the instantaneous FRS measurements in the central cross section of flame 1–3, zoomed in views of the region in Fig. 4 marked by red box.

4.2. Mean temperature distribution of the swirl flames

Figure 6 shows the mean temperature distributions of the FRS measurement results of flame 1–3. Each image displays the ensemble average of 50 single-shot images. It is clear from the mean FRS images that there are significant changes in temperature magnitude and flame structure with changing equivalence ratio Φ. The higher equivalence ratio results in the higher temperature intensity and wider flame area, as expected. From the nozzle at the bottom, all the averaged flames take the form of approximately symmetric, cone-shaped structures. This is different from the instantaneous FRS measurements in Fig. 3, of which the flames present asymmetric structures in the marginal cross sections due to the helical combustion flow generation. We conjecture that it is the random perturbations in the combustion fields that weaken the asymmetric distributions of the mean results.

To further qualify the axisymmetric distribution feature of the swirl flames, a simple data extraction algorithm is performed. The algorithm aims at extracting temperature distributions of seven cross sections at each centerline ($r = 0$ mm) and of central cross section S 0 at uniform radius $r = -15$ mm, -10 mm, -5 mm, 0 mm, 5 mm, 10 mm and 15 mm. It should be noticed that the centerline of seven cross sections locates at the surface perpendicular to the central cross section. Since the temperature distributions of flame 1–3 are similar and the temperature intensities of flame 3 are greater, we choose flame 3 as a representative analysis object in order to enhance contrast. Figure 7 shows a comparison of the profiles of the temperature distributions extracted from seven cross sections at each centerline and S 0 at seven uniform radius positions. The temperature distribution profiles at the same uniform radius are plotted designedly in the same color. An overall agreement between the temperature distributions presented in Figs. 7(a) and 7(b) is observed with some little differences among the seven sets of curves. The divergences noted at the same uniform

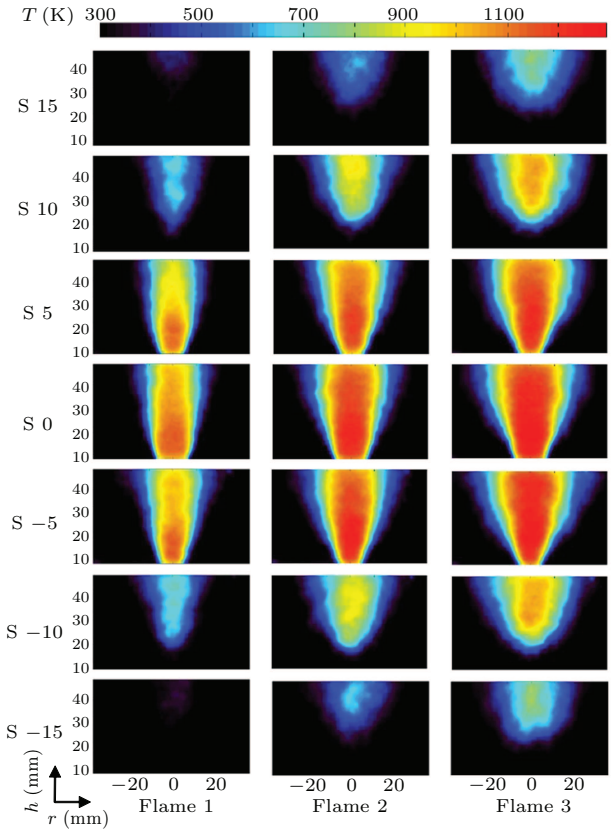


Fig. 6. Mean FRS temperature measurements in seven cross sections of flame 1–3.

radius positions are likely aroused by strong turbulence in the combustion field. Consequently, the axisymmetric distribution characteristic of the swirl flames can be determined.

Another interesting point for the mean temperature distributions of flame 1–3 is that the high temperature zones primarily exit in the central portion of the flames. This explains the primary role of the swirl generator to create an inner recirculation zone (IRZ), through which part of the burned mixture back towards the nozzle. This provides a hot combustion environment and a source of radicals, which improves ignition and thus enhances flame stabilization. Again, because of the axisymmetric distribution of the investigated swirl flames, the PDF profiles corresponding to the mean FRS images of flame 1–3 in the cross sections S 0, S 5, S 10 and S15 are calculated, as shown in Fig. 8. The horizontal axis is the temperature T and the vertical axis is the total count of pixel with specific temperature intensity. Regions related to the high temperature zone start around $T = 780$ K, as seen in the right peaks of the joint PDF profiles except that in Fig. 8(d). Apparently, higher equivalence ratio leads to higher temperature intensity and wider flame area. The peak around 460 K displayed in all PDF profiles corresponds to the flame boundary area of the main flame, where there exists the reaction zone with large temperature gradient.

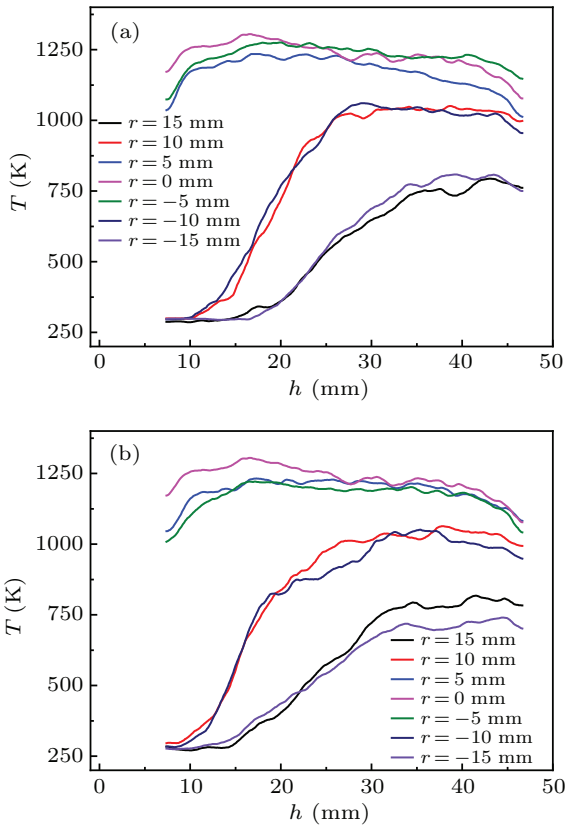


Fig. 7. The histograms of the temperature distributions extracted from (a) seven cross sections at each centerline and (b) S 0 at seven uniform radius positions.

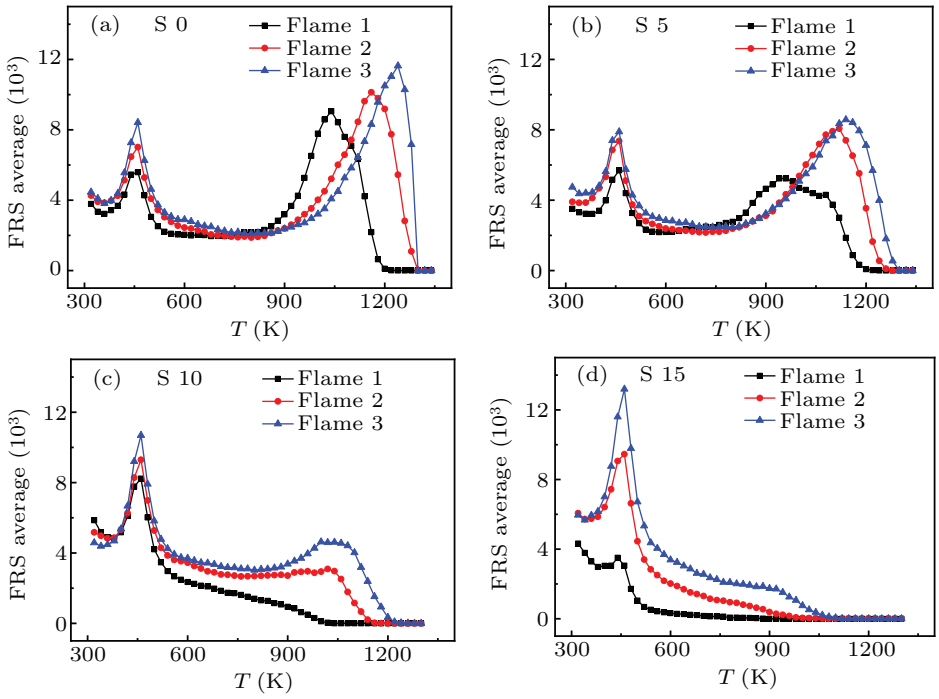


Fig. 8. The PDF profiles of mean FRS measurements of flame 1–3 at cross sections S 0, S 5, S 10, and S 15.

5. Summary

The characteristics of premixed swirl methane/air diffusion flames at atmospheric pressure have been studied by filtered Rayleigh scattering (FRS) thermometry. The equivalence ratio of three investigated flames covers a range from 0.67 to 0.83. Seven cross sections of each flame have been measured for detailed description of flame characteristics. The seven cross sections are placed parallel to each other along

the azimuthal direction with an adjacent separation distance of 5 mm. The instantaneous temperature distribution and flame shape have shown the features of typical rotational symmetric combustion field due to the helical mode and vortices breakdown phenomenon because of strong turbulence. The measured average flow field illustrates the mechanism of flame stabilization by the typical inner recirculation zone (IRZ), which is typical for swirl flames. The joint probability density function (PDF) profiles related to the mean temperature distributions quantify the effect of equivalence ratio on the thermochemical state of the flames. A particular focus of this study is the gradient intensity of the instantaneous FRS measurements for the characterization of the reaction zones. The gradient of the instantaneous FRS result demonstrates the reaction zone distributions and the heat release characteristics. The high gradient intensity indicates the presence of PVC (processing vortex core) at the boundary region, where a large part of heat release takes place.

The crucial weakness of the current FRS system is the repetition rate of the Nd:YAG laser source, which is only 10 Hz as used in this work. Higher sampling rate of the FRS system is preferable and crucial for the measurements of the temporal evolution process of flame characteristics. This problem could be solved in the future if high repetition rate laser with high pulse-energy becomes available.

Acknowledgement

Project supported by National Science and Technology Major Projects of China (Grant No. J2019-V-005-0096).

References

[1] Meier W, Duan X R and Weigand P 2005 *Proc. Combust. Inst.* **30** 835
[2] Meier W, Duan X R and Weigand P 2016 *Combus. Flame* **144** 225
[3] Meier W, Weigand P, Duan X R and Giezendanner-Thoben R 2007 *Combus. Flame* **150** 2
[4] Driscoll J F and Temme J 2011 *AIAA Aerospace Sciences Meeting*, January 4–7, 2011, Orlando, Florida
[5] Keller J J 1995 *AIAA J.* **33** 2280
[6] Paschereit C O, Gutmark E and Weisenstein W 1998 *Combust. Sci. Technol.* **138** 213
[7] Candel S 2002 *P. Combust. Inst.* **29** 1
[8] Lee J G and Santavicca D A 2003 *J. Propul. Power* **19** 735
[9] Syred N 2006 *Prog. Energy Combust. Sci.* **32** 93
[10] Anacleto P M, Fernandes E C, Heitor M V and Shtork S I 2003 *Combust. Sci. Technol.* **175** 1369
[11] Stöhr M, Sadanandan R and Meier W 2011 *Exp. Fluids* **51** 1153
[12] Stöhr M, Arndt C M amd Meier W 2015 *Proc. Combust. Inst.* **35** 3327
[13] Mounaim-Rousselle C, Landry L, Halter F and Foucher F 2013 *Proc. Combust. Inst.* **34** 2941
[14] Sadanandan R, Kutne P, Steinberg A and Meier W 2012 *Flow Turbulence Combust.* **89** 275
[15] McManus T A and Sutton J A 2019 *Appl. Opt.* **58** 2936
[16] Eckbreth A C 1996 *Laser Diagnostics for Combustion Temperature and Species* (Amsterdam: Gordon and Breach Publishers)
[17] Kohse-Höinghaus K, Barlow R S, Aldén M and Wolfrum J 2005 *Proc. Combust. Inst.* **30** 89
[18] Hofmann D and Leipert A 1996 *Symp. (Int.) Combust.* **26** 945
[19] Elliott G S, Glumac N, Carter C D and Nejad A S 1997 *Combust. Sci. Technol.* **125** 351
[20] Elliott G S, Glumac N and Carter C D 1999 *AIAA Aerospace Sciences Meeting and Exhibit*, January 11–14, 1999 Reno, Nevada
[21] Elliott G S, Glumac N and Carter C D 2011 *Meas. Sci. Technol.* **12** 452
[22] Most D and Leipertz A 2001 *Appl. Opt.* **40** 5379
[23] Most D, Dinkelacker F and Leipertz A 2002 *Proc. Combust. Inst.* **29** 2669
[24] Boguszko M and Elliott G S 2005 *Prog. Aerosp. Sci.* **41** 93
[25] Miles R B, Lempert W R and Forkey J N 2001 *Meas. Sci. Technol.* **12** R33
[26] Boguszko M and Elliott G S 2005 *Prog. Aerosp. Sci.* **41** 93
[27] McManus T A, Monje I T and Sutton J A 2019 *Appl. Phys. B* **125** 13
[28] McManus T A and Sutton J A 2020 *Exp. Fluids* **61** 134
[29] Bergmann V, Meier W, Wolf D and Stricker W 1985 *Appl. Phys. B* **66** 489
[30] Papageorge M J, McManus T A, Fuest F and Sutton J A 2014 *Appl. Phys. B* **115** 197
[31] McManus T A, Papageorge M J, Fuest F and J A Sutton 2015 *Proc. Combust. Inst.* **35** 1191
[32] Tenti G, Boley C and Desai R 1974 *Can. J. Phys.* **52** 285
[33] Young A T and Kattawar G W 1983 *Appl. Opt.* **22** 3668
[34] Pitz R, Cattolica R, Robben F and Talbot L 1976 *Combust. Flame* **27** 313
[35] Forkey J 1996 *Development and demonstration of fltered Rayleigh scattering: a laser based fow diagnostic for planar measurement of velocity, temperature and pressure* (Ph.D. Dissertation) (Princeton: Princeton University)
[36] Glassman I and Yetter R 2008 *Combustion* (New York: Academic Press)
[37] Li M, Yan B, Chen L and Chen S 2021 *Appl. Phys. B* **127** 80
[38] Sadanandan R, Kutne P, Steinberg A and Meier W 2012 *Flow Turbul. Combust.* **89** 275